ELSEVIER

Thermochimica Acta 377 (2001) 85–96

thermochimica acta

www.elsevier.com/locate/tca

Application of an extended Tool–Narayanaswamy–Moynihan model Part 1. Description of vitrification and complex heat capacity measured by temperature-modulated DSC

Stefan Weyer, Mikhail Merzlyakov, Christoph Schick*

Department of Physics, University of Rostock, 18051 Rostock, Germany

Received 23 February 2001; received in revised form 17 March 2001; accepted 20 March 2001

Abstract

Complex heat capacity in equilibrium can be considered as a compliance in the scheme of linear response. Nevertheless, often the Tool–Narayanaswamy–Moynihan (TNM) or the Kovacs–Aklonis–Hutchinson–Ramos (KAHR) models are used to describe complex as well as total heat capacity in the glass transition region. This is attractive because the TNM–KAHR models take into account the dependence of the relaxation time on temperature as well as fictive temperature and are able to handle non-equilibrium situations. A TNM-model extended by a non-Arrhenius temperature dependence of the relaxation time is applied to describe results from temperature-modulated DSC (TMDSC) measurements. The temperature dependence of the relaxation time, as introduced in the model, is independently determined by a VFTH-fit to heat capacity spectroscopic data in a wide frequency range. Finally, only the stretched exponential factor β and the non-linearity parameter x of the TNM-model must be adjusted to describe the measured curves reasonable well. The model is capable to describe all features of the heat capacities measured in TMDSC scan experiments in the glass transition region of polystyrene. This includes the curve shape, the frequency dependence of $T_g(\omega)$, the cooling rate dependence of $T_g(q_0)$ and possible interference between vitrification and dynamic glass transition. For the complex heat capacity in equilibrium, above vitrification, no influence of fictive temperature on the relaxation time was observed. Consequently, it can be considered as an equilibrium quantity.

Keywords: Tool–Narayanaswamy–Moynihan model; Glass transition; Temperature-modulated DSC (TMDSC); Polymers; Polystyrene (PS)

1. Introduction

Calorimetry is one of the most often applied experimental techniques to study the glass transition. Adiabatic and differential scanning calorimetry (DSC) are often used to study vitrification and relaxation processes in the glassy state [1]. Vitrification and devitrification means the change from the meta-stable liquid to the non-equilibrium glassy state and vice versa. The Tool–Narayanaswamy–Moynihan (TNM) and the Kovacs–Aklonis–Hutchinson–Ramos (KAHR) models are known as powerful tools to describe measured heat capacity on vitrification and devitrification under a wide variety of experimental conditions and thermal histories, see [2] and references therein. From dynamic (periodic) calorimetry complex heat capacity

* Corresponding author. Tel.: +49-381-498-1644; fax: +49-381-498-1626.
E-mail address: christoph.schick@physik.uni-rostock.de (C. Schick).

0040-6031/01/$ – see front matter
PII: S0040-6031(01)00543-3

is available. Also with these techniques glass transition was studied first. Gobrecht et al. used temperature modulated DSC (TMDSC) as early as in 1971 to measure frequency dependence of complex heat capacity at the glass transition of selenium [3]. With introduction of the 3ω technique by Birge in 1986 complex heat capacity was available in a wide frequency range [4]. The results obtained by the 3ω technique are often described as a compliance in the framework of linear response [5].

While the TNM–KAHR models take into account the acceleration of the relaxation due to the deviation from the equilibrium, complex heat capacity is often considered as an equilibrium quantity. Nevertheless, there are several attempts to describe complex heat capacity by means of the TNM–KAHR [6–10] or similar models [11–14]. The basic features of complex heat capacity, step in real and peak in imaginary part as well as a shift with frequency, are well reproduced by these approaches. But a detailed comparison with experimental data especially in the region near vitrification temperature (conventional, thermal glass transition) is still missing. In the first part of this paper, we will present such a comparison based on the TNM-model including non-Arrhenius (VFTH) temperature dependence of the equilibrium relaxation time [15–17]. The model will not be used to determine the relevant parameters applying a fitting procedure. The parameters will be determined, as far as possible, by independent measurements like heat capacity spectroscopy in a wide frequency range [18]. Finally, a single set of parameters is used to describe measurements of total (conventional, measured by DSC) heat capacity as well as real and imaginary part of complex heat capacity on cooling and heating through the glass transition of polystyrene (PS). In the second part of this paper [19], we will compare predictions of the model with experimental results for more complex quantities, like modulus and phase of higher harmonics in the measured heat flow rate [20].

2. Experimental

2.1. DSC measurements

The technique of TMDSC and the necessary data treatments are described elsewhere [21–25]. The 168N polystyrene (PS) was from BASF ($\rho = 1.047$ g/cm^3; $M_n = 95{,}000$ g/mol; $M_W = 270{,}000$ g/mol). DSC measurements were performed to determine conventional or $C_{p\ \mathrm{total}}$ and TMDSC to determine complex heat capacity. Perkin-Elmer Instruments DSC2 and Setaram DSC121 were used. The sample masses were $m_{PS} = 14$ and 230 mg, respectively. The temperature scale of the calorimeters was calibrated in DSC mode at zero heating rate according to the recommendations of GEFTA [26] by indium and lead, and was checked in the TMDSC mode by the smectic-to-nematic transition of 8OCB [27,28]. The determination of complex heat capacity, especially the correction of the measured phase angle, was performed as described in [29]. The TMDSC experiments were carried out with sinusoidal modulation with temperature amplitude $A_T = 0.5$ K and modulation period $t_p = 60$ s. The underlying cooling rate was varied between $q_0 = 1$K/min and $q_0 = 0.001$ K/min.

2.2. Definition of experimental conditions

From shear spectroscopy [30] it is well known that vitrification of the sample during the dynamic measurement has some impact on the measured compliance or modulus. The problem arises when the dynamic measurement is performed at low frequencies (mHz) and the sample is cooled fast. In case of TMDSC, we have always to consider this interference because measurements are performed at low frequencies (mHz) and cooling is relatively fast (K/min). From TMDSC measurements we yield simultaneous information about the two aspects of glass transition — thermal glass transition (vitrification) and dynamic glass transition (relaxation process). They are the responses of the sample on two independent perturbations — thermal glass transition due to underlying cooling rate and dynamic glass transition due to temperature modulation (frequency dependent), see Fig. 1.

Under measuring conditions as in Fig. 1, which are typical for TMDSC, the step and the peak in complex heat capacity (dynamic glass transition) are not well separated from vitrification (step in $C_{p\ \mathrm{total}}$). To study the dynamic glass transition in equilibrium the difference between both has to be enlarged.

To shift the dynamic glass transition with respect to vitrification, cooling rate and/or frequency can be

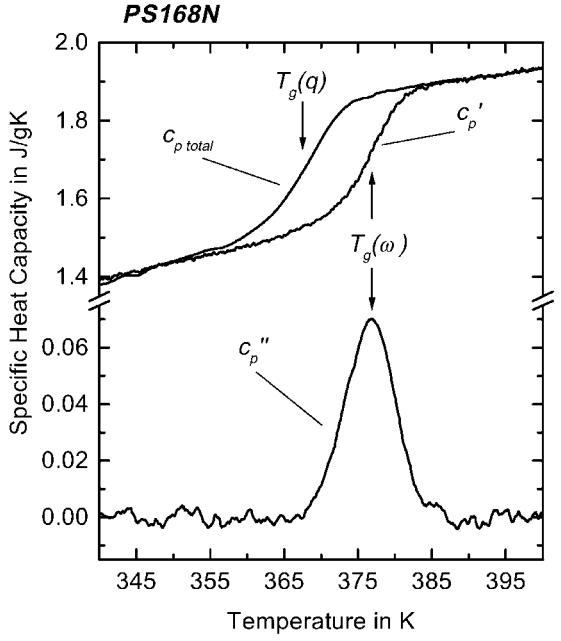

Fig. 1. Specific heat capacity for polystyrene measured by TMDSC ($t_p = 60$ s, $A_T = 0.5$ K, $q_0 = -0.25$ K/min). Perkin-Elmer Instruments DSC2 and Setaram DSC121.

varied [18,31–34]. We have fixed the dynamic glass transition temperature using a fixed frequency of $f = 0.017$ Hz (period $t_p = 60$ s). Vitrification was shifted by varying underlying cooling rate, see Figs. 2 and 3. This way we define the experimental conditions were the dynamic glass transition is not or only little influenced by vitrification in the TMDSC measurements discussed here.

The measurements show the expected interference between vitrification and dynamic glass transition. For decreasing cooling rates, vitrification is shifted to lower temperatures, the step in real part of complex heat capacity becomes sharper and more symmetric. This can also be seen in the phase angle δ_S. For decreasing cooling rate δ_S fits better to a symmetric Gaussian (Fig. 3).

For an underlying cooling rate of $q_0 = -0.001$ K/min vitrification is reasonable well separated from the dynamic glass transition. Only at temperatures below $T = 372$ K, what is practically outside the step in modulus and the peak in phase of complex heat capacity, vitrification overlaps with the dynamic glass transition. Under these measuring conditions the

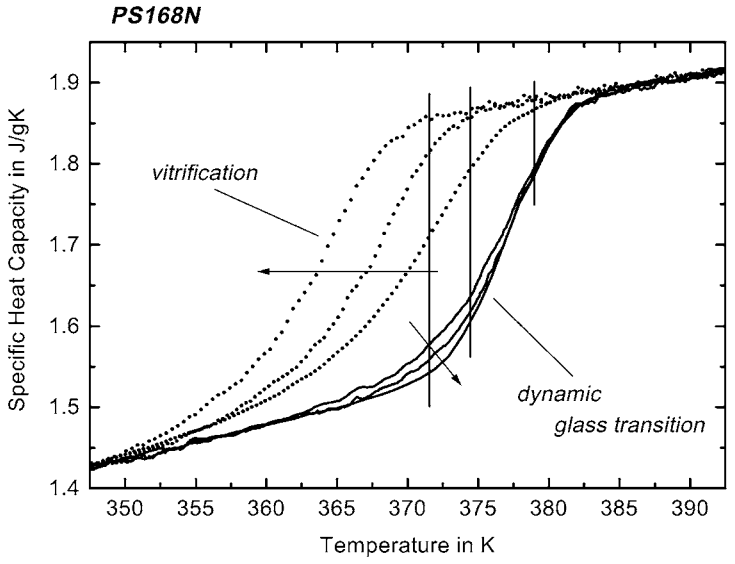

Fig. 2. Modulus of complex specific heat capacity (dynamic glass transition) and total heat capacity (vitrification) from TMDSC measurements at fixed modulation frequency and different underlying cooling rates ($t_p = 60$ s, $A_T = 0.5$ K, $q_0 = -1, -0.06, -0.001$ K/min). The arrows indicate decreasing cooling rate. Vitrification at $q_0 = -0.001$ K/min was not measured. The curve shown is the curve measured at $q_0 = -0.06$ K/min and shifted according to the activation diagram [32]. Vertical lines indicate the beginning of vitrification. Perkin-Elmer Instruments DSC2 and Setaram DSC121.

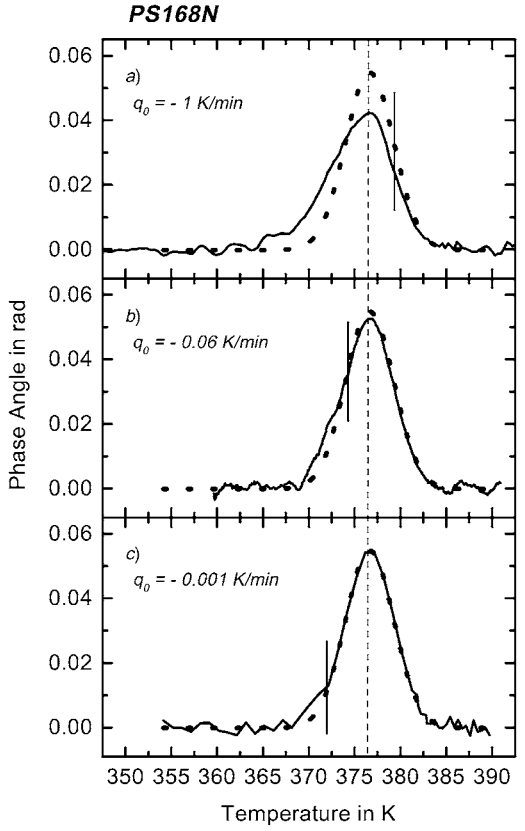

Fig. 3. Phase angle of complex heat capacity for a fixed modulation frequency and different underlying cooling rates ($t_p = 60$ s, $A_T = 0.5$ K, $q_0 = -1$, -0.06, -0.001 K/min). The short vertical lines indicate the beginning of vitrification, same as in Fig. 2. A Gaussian was fitted on curve c in the temperature range above the dotted line. The same Gaussian is shown in the other graphs, thick dotted curve, to make the changes in curve shape visible. The dashed line marks the maximum of curve c. Perkin-Elmer Instruments DSC2.

dynamic glass transition appears in equilibrium and it can be checked whether or not it can be described as an equilibrium process.

3. Extended Tool–Narayanaswamy–Moynihan model

An extended TNM-model, discussed in detail by Donth and coworkers [17,35], was used to describe vitrification and dynamic glass transition as well as possible interferences between both [6,36]. Not only the normalised heat capacities were determined but the corresponding heat flow rates for the different experimental conditions were calculated to be able to compare the results from the model calculations with experimental results. For both, the measured and the calculated heat flow rates, the same data treatment algorithm, as usual in TMDSC, was applied to obtain total and complex heat capacity. The whole scheme, briefly described below [2], was implemented in a *Mathlab*™ program.

In order to characterise the actual thermodynamic state Tool introduced the fictive temperature T_f, which supplies information about free volume or structure [37–39]:

$$T_f(t) = T_0 + \int_{t_0}^{t} dT' \times \{1 - \phi(\Delta\zeta)\}, \quad T' = T(t'). \tag{1}$$

One starts in equilibrium at $T_0 = T(t_0)$ and integrates over the whole thermal history. According to Moynihan et al. [40,41] the Kohlrausch–Williams–Watt (KWW) function [42,43] can be chosen as response function:

$$\phi = \exp\{-(\Delta\zeta)^{\beta}\}, \quad 0 < \beta \leq 1, \tag{2}$$

where β describes the non-exponential character of the relaxation process. The so-called Kohlrausch exponent is considered in a first approximation to be temperature independent, see also [14]. One introduces a dimensionless material time difference $\Delta\zeta$ in order to linearize the relaxation process and to be able to apply linear response approach:

$$\Delta\zeta = \zeta(t) - \zeta(t') = \int_{t'}^{t} \frac{dt'}{\tau_{TNM}}, \tag{3}$$

where the relaxation time τ_{TNM} counts the time of an internal clock. The structural relaxation in terms of τ_{TNM} is controlled by both the actual temperature T and the fictive temperature T_f. Narayanaswamy weighted their influence in a mixing approach with the non-linearity parameter x [44], and Scherer [15] replaced the Arrhenius-like temperature dependence of the relaxation time by a more realistic non-linear function. In the following, we use the well-known Vogel–Fulcher–Tamman–Hesse (VFTH)

equation [45–47] to take into account the non-linear behaviour:

$$\log\omega = A + \frac{B}{T - T_\infty} = \frac{1}{2.3026} \times \left\{ -\ln\tau_0 + \frac{-\Delta h^*}{R \times (T - T_\infty)} \right\}. \quad (4)$$

Then, we get for the relaxation time

$$\tau_{\mathrm{TNM}} = \exp\left\{ \ln\tau_0 + \frac{\Delta h^* \times x}{R \times (T - T_\infty)} + \frac{\Delta h^* \times (1 - x)}{R \times (T_\mathrm{f} - T_\infty)} \right\}, \quad 0 < x \leq 1. \quad (5)$$

Finally, the calculation of fictive temperature takes place recursive in steps of time/temperature, where time/temperature history is broken into suitable intervals:

$$T_{\mathrm{f},n} = T_0 + \sum_{i=1}^{n} \Delta T_i \times \left[1 - \exp\left\{ -\left(\sum_{j=1}^{n} \frac{\Delta t_j}{\tau_{\mathrm{TNM},j}} \right)^{\beta} \right\} \right]. \quad (6)$$

Like mentioned above, our aim is the comparison of TNM-model calculations and results from TMDSC measurements. That is why we consider a temperature-time profile as commonly used in TMDSC:

$$T(t) = T_0 + q_0 \times t + A_T \times \sin(\omega \times t). \quad (7)$$

In Fig. 4, the temperature profile and the evolution of the fictive temperature on cooling is shown.

At high temperatures fictive temperature and temperature coincide. For sake of clarity, both curves are shifted vertically as indicated in Fig. 4. With decreasing temperature the amplitude of oscillations in fictive temperature decreases, indication of the dynamic glass transition, and disappear before fictive temperature becomes constant as common for vitrification.

Next, in order to obtain the heat flow rates from the model calculations, which equal the time derivative of enthalpy, fictive temperature was transferred into enthalpy. As common, enthalpy as function of temperature $H(T)$ can be defined as [48–50]

$$H(T) = H_\infty(T) + \delta(T), \quad (8)$$

with equilibrium enthalpy $H_\infty(T)$ and excess enthalpy $\delta(T)$. Like illustrated in Fig. 4 fictive temperature can

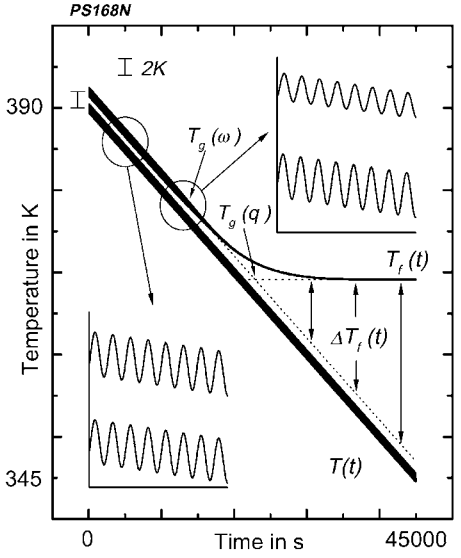

Fig. 4. Temperature, $T(t)$, and fictive temperature, $T_\mathrm{f}(t)$, vs. time on cooling ($t_\mathrm{p} = 60$ s, $A_T = 0.5$ K, $q_0 = -0.06$ K/min); TNM-parameters: $\ln(\tau_0/s) = -28.02$, $\Delta h^*/R = 1305$ K, $T_\infty = 333$ K, $x = 0.22$, $\beta = 0.56$.

be expressed similar way as

$$T_\mathrm{f}(t) = T(t) + \Delta T_\mathrm{f}(t). \quad (9)$$

Assuming temperature independent heat capacities in the liquid, $C_{p\mathrm{l}}$, and in the glassy state, $C_{p\mathrm{g}}$, with ΔC_p as the difference between both yields [6,36]

$$H(T, T_\mathrm{f}) = C_{p\mathrm{l}} \times T + \Delta C_p \times (T_\mathrm{f} - T). \quad (10)$$

Finally, the heat flow rate HF is defined as the time derivative of enthalpy and given by Eq. (11):

$$\mathrm{HF} = \frac{\mathrm{d}H(T, T_\mathrm{f})}{\mathrm{d}t} = C_{p\mathrm{l}} \times \frac{\mathrm{d}T}{\mathrm{d}t} + \Delta C_p \times \left(\frac{\mathrm{d}T_\mathrm{f}}{\mathrm{d}t} - \frac{\mathrm{d}T}{\mathrm{d}t} \right). \quad (11)$$

We define $\mathrm{d}T/\mathrm{d}t \equiv q(t)$ and $\mathrm{d}T_\mathrm{f}/\mathrm{d}t \equiv q_\mathrm{f}(t)$. With $C_{p\mathrm{l}} - \Delta C_p = C_{p\mathrm{g}}$, Eq. (11) results in

$$\mathrm{HF} = C_{p\mathrm{g}} \times q + \Delta C_p \times q_\mathrm{f}. \quad (12)$$

Eq. (12) is given in time domain. After Fourier transformation we get

$$A^*_{\mathrm{HF}}(\omega) = C_{p\mathrm{g}} \times A^*_\mathrm{q}(\omega) + \Delta C_p \times A^*_{\mathrm{q_f}}(\omega), \quad (13)$$

where A^* means complex amplitudes, see below. From the complex heat flow amplitude A^*_{HF}, which is

available from the TNM-model, Eq. (13), as well as for real measurements, complex heat capacity, $C_p^*(\omega)$, can be obtained from

$$C_p^*(\omega) = \frac{A_{\mathrm{HF}}^*(\omega)}{A_{\mathrm{q}}^*(\omega)} \tag{14}$$

and total heat capacity from

$$C_{p\,\mathrm{total}} = \frac{\langle \mathrm{HF} \rangle}{q_0} = C_{p\mathrm{g}} + \Delta C_p \times \frac{\langle q_\mathrm{f} \rangle}{\langle q \rangle} = C_{p\mathrm{g}} + \Delta C_p \times \frac{\langle \mathrm{d}T_\mathrm{f} \rangle}{\langle \mathrm{d}t \rangle}, \tag{15}$$

where ω is the angular frequency; A_{HF}^* the Fourier image of heat flow rate which includes amplitude and phase. Therefore, this is like A_{q}^* and $A_{\mathrm{q_f}}^*$ a complex value; A_{q}^* the Fourier image of heating rate, the time derivative of temperature; $A_{\mathrm{q_f}}^*$ the Fourier image of the time derivative of fictive temperature; ΔC_p the increment in heat capacity between glassy and liquid state; $C_{p\mathrm{g}}$ the heat capacity of the glass; $\langle \cdot \rangle$ the average over one modulation period.

Basically, the complex heat flow rate amplitude consists of two components as shown in Fig. 5. Namely, $C_{p\mathrm{g}} \times A_{\mathrm{q}}^*$ and $\Delta C_p \times A_{\mathrm{q_f}}^*$. In case the phase of the heating rate equals zero the first term becomes real valued, see Fig. 5. The second term originate from the TNM-model and includes all time dependence of the heat capacity. This yields the phase $\delta_{A_{\mathrm{q_f}}^*}$. The complex heat flow rate amplitude A_{HF}^* equals the sum of both contributions in complex plane.

Now one can compare measured complex heat capacity with that from Eq. (14) either in terms of imaginary and real part or in terms of modulus and argument of complex heat capacity. We will present our results in the last form because often the so called reversing heat capacity [21] is available from the instruments which equals the modulus of complex heat capacity

$$|C_p^*(\omega)| = \mathrm{abs}\left|\left(\frac{A_{\mathrm{HF}}{}^*(\omega)}{A_{\mathrm{q}}^*(\omega)}\right)\right| \tag{16}$$

and

$$\delta_{\mathrm{S}}(\omega) = \arg\left(\frac{A_{\mathrm{HF}}^*(\omega)}{A_{\mathrm{q}}^*(\omega)}\right). \tag{17}$$

In order to obtain heat flow rate curves HF(t) from the model calculations suitable for data evaluation in terms of complex heat capacity one has to take care not to violate the conditions of linearity and stationarity of the response [13,14,51,52]. Therefore, temperature amplitude and cooling rate must be small enough. To limit the uncertainties due to the Fourier transform we need a certain number of points per modulation period, ca. 30. Consequently, for low cooling rates a large number of points must be calculated at a given frequency. The following calculations were performed.

As can be seen from Table 1 computation time increases quadratic with decreasing cooling rate. To keep computation time in a reasonable limit at cooling rate $q_0 = -0.001$ K/min the temperature profile was divided in two parts. First, down to $T = 378$ K the cooling rate was $q_0 = -0.06$ K/min. Above this temperature the sample is still in equilibrium because no

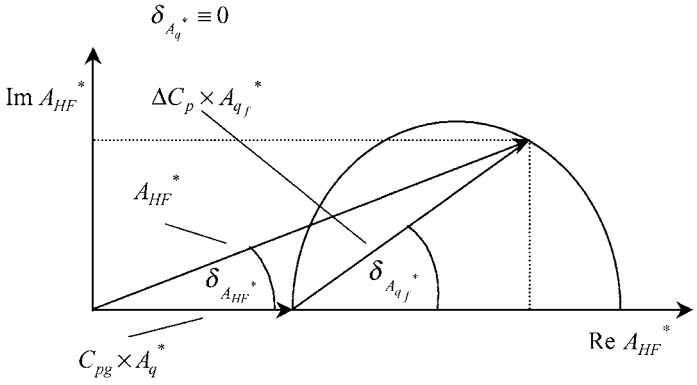

Fig. 5. Schematic diagram of vector addition of Fourier images contributing to the complex amplitude of heat flow rate $A_{\mathrm{HF}}{}^*$ in a polar plot.

Table 1
Cooling rate, q_0, temperature range, ΔT, and number of points per period for the model calculations[a]

q_0 (K/min)	ΔT (K)	Points per period	Number of points	Calculation time
−1	40	30	1200	∼1 min
−0.06	40	30	20000	∼4.5 h
−0.06, −0.001	7, 13	30, 20	3500, 263500	∼32 days

[a] The resulting total number of points and the corresponding computation time (Pentium II 350 MHz with 128 M bytes RAM) are given in the last two columns, respectively.

vitrification occurs. Therefore, the cooling rate $q_0 = -0.06$ K/min had no influence on complex heat capacity. Next, the cooling rate of $q_0 = -0.001$ K/min was used for the temperature region of the glass transition, $T = 378$–365 K.

4. Results

In order to obtain complex heat capacity from the extended TNM-model, Eqs. (1)–(17), one has to determine τ_0, $\Delta h^*/R$, T_∞, β and x. The first three are independently available from heat capacity spectroscopy, see below, while the last two will be determined by a fitting procedure.

The parameters τ_0, $\Delta h^*/R$ and T_∞ can be obtained from a VFTH-fit to dynamic glass transition temperatures in a wide frequency range. The combination of 3ω, photo-acoustic (PA), AC-calorimetric (AC), and TMDSC measurements allows for heat capacity spectroscopy in a frequency range of seven orders of magnitudes for PS [18], see Fig. 6.

The data are fitted with the VFTH-equation, Eq. (4). The parameters given in Fig. 6 equal $\ln(\tau_0/s) = -28.02$, $\Delta h^*/R = 1305$ K, $T_\infty = 333$ K. By using these parameters and varying β and x we adjusted the heat capacities from the model calculation to the measured $C_{p\,\mathrm{total}}$ (DSC) curves on cooling and heating with $q_0 = \pm 1$ K/min. For the calculation we assume temperature independent heat capacities of the glassy

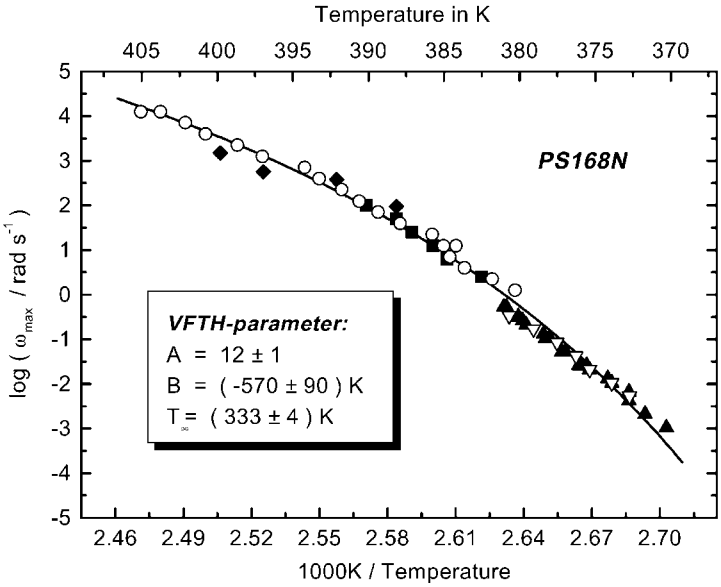

Fig. 6. Activation diagram for polystyrene obtained from different calorimetric methods: (◆) — photo-acoustic [53]; (○) — 3ω [18,54]; (■) — AC-calorimetry [55]; (▽) — TMDSC multi frequency analysis [56]; (▲) — TMDSC [18,54]. Solid line is VFTH-curve with parameters $A = 12 \pm 1$, $B = (-570 \pm 90)$ K and $T_\infty = (333 \pm 4)$ K.

and the liquid state. Because this assumption is not valid for the measurements we use, as common, a reduced heat capacity for comparison

$$C_{p\,\mathrm{red}} = \frac{C_p(T) - C_{pg}(T)}{C_{pl}(T) - C_{pg}(T)}. \tag{18}$$

The phase δ_S was calculated with Eq. (17) for the actual values of heat capacity as shown in Fig. 5.

Using the parameters obtained from the VFTH-fit and $x = 0.22$ and $\beta = 0.56$ results in the curves shown in Fig. 7. The agreement between the measured and calculated heat capacities, $C_{p\,\mathrm{total}}, |C_p^*|$, as well as between the phase angles, δ_S, is reasonable. Only at heating around 365 K an significant deviation between measured and calculated $C_{p\,\mathrm{total}}$ can be seen. This seems to be an intrinsic problem of the TNM-model and is reported several times [9,50,57].

In Fig. 7, we used experimental conditions where dynamic glass transition and vitrification interferes. Especially for the heating curve the well-known sharpening of the dynamic glass transition [12,31,33,58] can be seen. The calculation nicely reproduce this effect in modulus and phase of complex heat capacity.

To show the effect of non-Arrhenius behaviour of τ_0 on the results of the model, calculations assuming Arrhenius like behaviour of τ_0, which means $T_\infty = 0$ K, were performed. The results are compared with the measured data in Fig. 8. As can be seen the agreement between calculated and measured curves, especially for the phase angle, is not as good as in Fig. 7. The situation becomes much worse if the same values as in Fig. 7 are used for x and β. To be able to describe the measured heat capacities in a wider frequency and cooling rate range we continue with

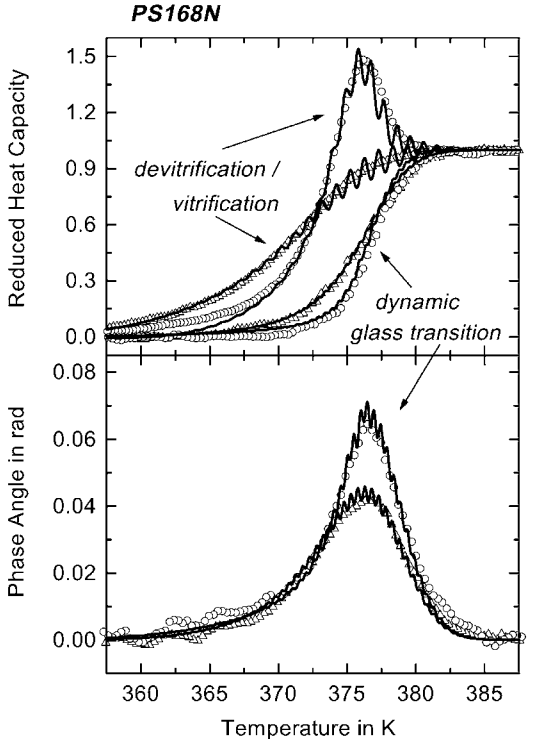

Fig. 7. Reduced heat capacity and phase angle of TMDSC — measurements ($t_p = 60$ s, $A_T = 0.5$ K, $q_0 = \pm 1$ K/min), Perkin-Elmer Instruments DSC2 and Setaram DSC121. (△) — TMDSC on cooling; (○) — TMDSC on heating, solid line — TNM-model; TNM-parameters: $\ln(\tau_0/s) = -28.02$, $\Delta h^*/R = 1305$ K, $T_\infty = 333$ K, $x = 0.22$, $\beta = 0.56$.

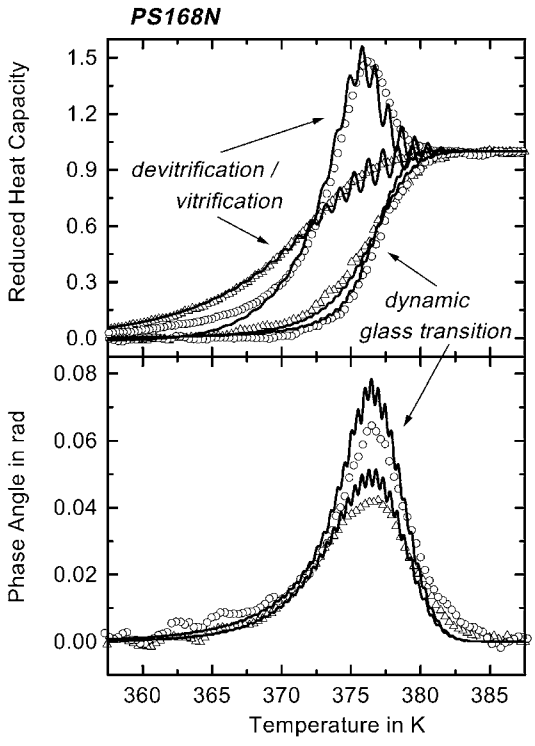

Fig. 8. Reduced heat capacity and phase angle of TMDSC — measurements ($t_p = 60$ s, $A_T = 0.5$ K, $q_0 = \pm 1$ K/min), Perkin-Elmer Instruments DSC2 and Setaram DSC121. (△) — TMDSC on cooling; (○) — TMDSC on heating, solid line — TNM-model; TNM-parameters: $\ln(\tau_0/s) = -243.3$, $\Delta h^*/R = 92500$ K, $T_\infty = 0$ K, $x = 0.44$, $\beta = 0.63$.

the extended TNM-model, Eq. (5), taking into account the non-Arrhenius behavior of τ_0.

As shown in Fig. 7 the model is capable to reproduce the influence of partial vitrification and devitrification. In Fig. 9, calculated data for different cooling rates are shown and compared with the measured data, same as in Figs. 2 and 3.

With decreasing cooling rate vitrification is shifted towards lower temperatures and vitrification and dynamic glass transition are better separated, see also Figs. 2 and 3. Again the sharpening of complex heat capacity on decreasing cooling rate is nicely reproduced by the model calculation. For cooling rates of $q_0 = -0.001$ K/min no significant overlap of dynamic glass transition and vitrification occurs. This allows us to address the question whether or not complex heat capacity can be described as an equilibrium quantity [14]. Therefore, we performed model calculations using the whole set of parameters as in all other calculations and we calculated complex heat capacity setting $x = 1$. Doing so we assume that there is no influence of the non-equilibrium on the relaxation time. In other words, we try to describe the dynamic glass transition as an equilibrium relaxation process. The results of these calculations for cooling rates $q_0 = -1$ and -0.001 K/min are shown in Fig. 10.

With $x = 0.22$ all measured curves are described reasonable well, see Fig. 7. Assuming $x = 1$ yields, of course, totally wrong curves for vitrification. For the dynamic glass transition, seen in the complex heat

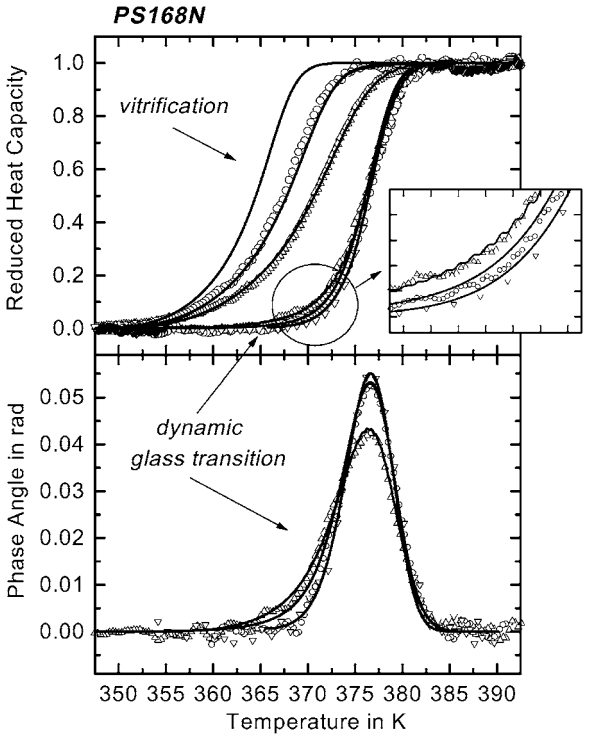

Fig. 9. Reduced heat capacity and phase angle of TMDSC — measurements at different cooling rates ($t_p = 60$ s, $A_T = 0.5$ K), Perkin-Elmer Instruments DSC2 and Setaram DSC121. (△) — $q_0 = -1$ K/min; (○) — $q_0 = -0.06$ K/min; (▽) — $q_0 = -0.001$ K/min, solid line — TNM-model. For the sake of clarity all calculated curves are smoothed over one modulation period. TNM-parameters: $\ln(\tau_0/s) = -28.02$, $\Delta h^*/R = 1305$ K, $T_\infty = 333$ K, $x = 0.22$, $\beta = 0.56$.

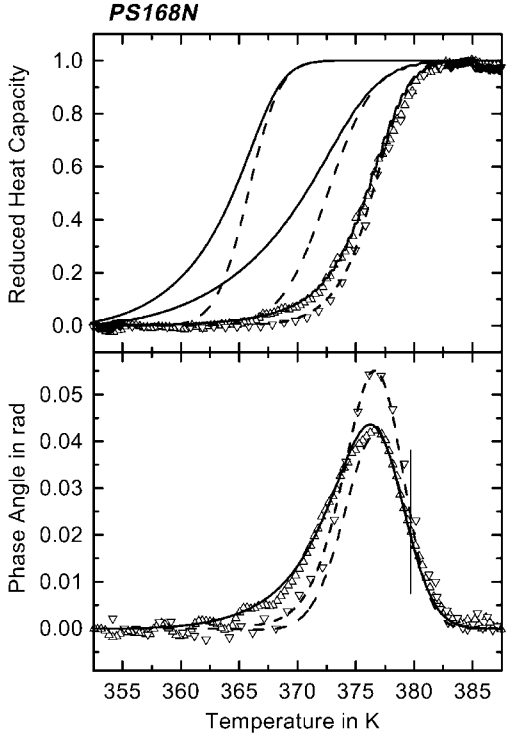

Fig. 10. Reduced heat capacity and phase angle of TMDSC — measurements and model calculations ($t_p = 60$ s, $A_T = 0.5$ K) at cooling rates (△) — $q_0 = -1$ K/min; (▽) — $q_0 = -0.001$ K/min, Perkin-Elmer Instruments DSC2, and line — TNM-model. For the sake of clarity, all calculated curves are smoothed over one modulation period. TNM-parameters: $\ln(\tau_0/s) = -28.02$, $\Delta h^*/R = 1305$ K, $T_\infty = 333$ K, $\beta = 0.56$, $x = 0.22$ (solid line) and $x = 1.00$ (dashed line).

capacity, the situation is different. For the cooling rate $q_0 = -0.001$ K/min there is no difference for the calculation with $x = 0.22$ and that with $x = 1$ and both equal the measured heat capacity. As shown above the measurement at $q_0 = -0.001$ K/min is performed in the equilibrium state of the super-cooled melt. Therefore, we do not expect an influence of the non-equilibrium which is taken into account in the TNM-model and weighted by the parameter x.

For cooling rate $q_0 = -1$ K/min and $x = 1$ the measured curves are also adequately described as long as the measurement is performed in equilibrium above 378 K, indicated by the vertical line. At lower temperatures, when vitrification starts, deviations from the measured curves can be observed. The modulus of heat capacity then follows the curve for the $q_0 = -0.001$ K/min measurement indistinguishably. The differences are more pronounced in the phase angle. Down to 378 K there is no difference between the curves for $x = 0.22$ and $x = 1$, as expected for a measurement in equilibrium. Below this temperature, when vitrification starts, the peak in the phase for $q_0 = -1$ K/min and $x = 1$ becomes smaller than the measured and that calculated with $x = 0.22$. The change in the peak shape of the phase angle may be partly due to the violation of the condition of stationarity at this relatively high cooling rate [13,51,52]. This will be studied in more detail in the second part of this paper. Interestingly, the extended TNM-model is capable to describe such complex situations accurately.

Next, we compare the frequency and cooling rate dependence of dynamic glass transition and vitrification [32], respectively, for measured and calculated curves.

The frequency dependence of the dynamic glass transition for both measured and calculated points is obviously described by the VFTH-curve which was derived from the measured points in a wider frequency range, see Fig. 6, and used for the model calculations. The cooling rate dependence of vitrification can, as discussed in [32,34], also be described by a VFTH-curve with the same temperature asymptote T_∞ but vertically shifted by $\log Y = 1.5$ as can be seen in Fig. 11. The shift for the model calculation is within experimental uncertainties a little higher than that for the measured data, $\log Y = 1.3$ [32].

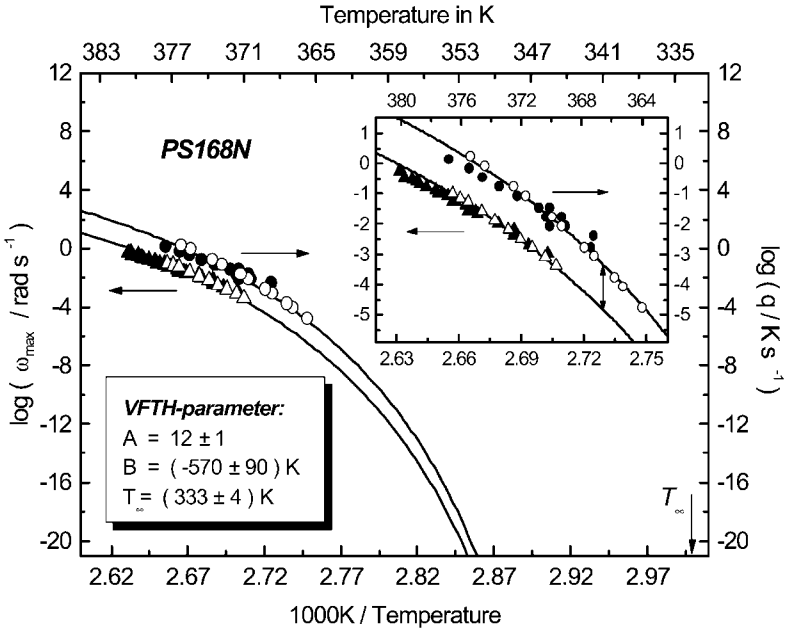

Fig. 11. Activation diagram for polystyrene from TMDSC (▲) and DSC (●) measurements as well as TNM-model calculations (△, ○). Triangles lie on VFTH-curve with parameters $A = 12 \pm 1$, $B = (-570 \pm 90)$ K and $T_\infty = (333 \pm 4)$ K. Circles lie on VFTH-curve with the same parameters but shifted in vertical direction by $\log Y = 1.5$ indicated by the vertical double-arrow.

5. Conclusion

The TNM-model extend by a non-Arrhenius temperature dependence of the relaxation time describes reasonable well all features of the heat capacities measured in TMDSC scan experiments in the glass transition range of polystyrene. This includes the curve shape, the frequency dependence of $T_g(\omega)$, the cooling rate dependence of $T_g(q_0)$ and possible interference between vitrification and dynamic glass transition. The ratio between frequency and cooling rate, experimentally determined previously [32], is confirmed by the model. The parameters of the VFTH-equation, to describe the temperature dependence of the relaxation time, τ, can be independently determined from heat capacity spectroscopy in a wide frequency range. Consequently, only the stretched exponential parameter β and the non-linearity parameter x in the TNM-model have to be determined by a fitting procedure. Complex heat capacity in equilibrium, above vitrification, can be considered as an equilibrium quantity.

Acknowledgements

This work was supported in part (S.W.) by the government of Mecklenburg-Vorpommern. M.M. acknowledges support by Perkin-Elmer Instruments.

References

[1] H. Suga, M. Oguni, in: T.M. Letcher (Ed.), Chemical Dynamics: Chemistry for the 21th Century (IUPAC), Blackwell Science, Oxford, 1999, p. 227.
[2] I.M. Hodge, J. Non-Cryst. Solids 169 (1994) 211.
[3] H. Gobrecht, K. Hamann, G. Willers, J. Phys. E: Sci. Instr. 4 (1971) 21.
[4] N.O. Birge, Phys. Rev. B34 (1986) 1631.
[5] R. Kubo, Rep. Prog. Phys. 29 (1966) 255.
[6] S.L. Simon, G.B. McKenna, J. Chem. Phys. 107 (1997) 8678.
[7] S.L. Simon, G.B. McKenna, Thermochim. Acta 348 (2000) 77.
[8] J.M. Hutchinson, S. Montserrat, J. Therm. Anal. 47 (1996) 103.
[9] J.M. Hutchinson, S. Montserrat, this issue.
[10] E. Flikkema, G.A. Vanekenstein, G. ten Brinke, Macromolecules 31 (1998) 892.
[11] J.E.K. Schawe, S. Theobald, J. Non-Cryst. Solids 235 (1998) 496.
[12] J.E.K. Schawe, Colloid Polym. Sci. 276 (1998) 565.
[13] Y.H. Jeong, I.K. Moon, Phys. Rev. B52 (1995) 6381.
[14] I.K. Moon, Y.H. Jeong, this issue.
[15] G.W. Scherer, J. Am. Ceram. Soc. 67 (1984) 504.
[16] I.M. Hodge, Macromolecules 20 (1987) 2897.
[17] E. Hempel, S. Kahle, R. Unger, E. Donth, Thermochim. Acta 329 (1999) 97.
[18] S. Weyer, A. Hensel, J. Korus, E. Donth, C. Schick, Thermochim. Acta 305 (1997) 251.
[19] S. Weyer, M. Merzlyakov, C. Schick, in preparation.
[20] C. Schick, M. Merzlyakov, A. Hensel, J. Chem. Phys. 111 (1999) 2695.
[21] M. Reading, Trends Polym. Sci. 8 (1993) 248.
[22] J.E.K. Schawe, Thermochim. Acta 260 (1995) 1.
[23] J.E.K. Schawe, Thermochim. Acta 261 (1995) 183.
[24] J.E.K. Schawe, G.W.H. Höhne, Thermochim. Acta 287 (1996) 213.
[25] B. Wunderlich, Y.M. Jin, A. Boller, Thermochim. Acta 238 (1994) 277.
[26] S.M. Sarge, W. Hemminger, E. Gmelin, G.W.H. Höhne, H.K. Cammenga, W. Eysel, J. Therm. Anal. 49 (1997) 1125.
[27] A. Hensel, C. Schick, Thermochim. Acta 305 (1997) 229.
[28] C. Schick, U. Jonsson, T. Vassilev, A. Minakov, J. Schawe, R. Scherrenberg, D. Lörinczy, Thermochim. Acta 347 (2000) 53.
[29] S. Weyer, A. Hensel, C. Schick, Thermochim. Acta 305 (1997) 267.
[30] W. Sommer, Kolloid-Zeitschrift 167 (1959) 97.
[31] A. Boller, C. Schick, B. Wunderlich, Thermochim. Acta 266 (1995) 97.
[32] A. Hensel, C. Schick, J. Non-Cryst. Solids 235–237 (1998) 510.
[33] J.E.K. Schawe, J. Therm. Anal. 47 (1996) 475.
[34] E. Donth, J. Korus, E. Hempel, M. Beiner, Thermochim. Acta 305 (1997) 239.
[35] E. Hempel, S. Kahle, R. Unger, E. Donth, Thermochim. Acta 330 (1998) 97.
[36] S.L. Simon, G.B. McKenna, Thermochim. Acta 307 (1997) 1.
[37] A.Q. Tool, C.G. Eichlin, J. Am. Ceram. Soc. 14 (1931) 276.
[38] A.Q. Tool, J. Am. Ceram. Soc. 29 (1946) 240.
[39] A.Q. Tool, J. Am. Ceram. Soc. 31 (1948) 177.
[40] C.T. Moynihan, et al., Ann. N.Y. Acad. Sci. 279 (1976) 15.
[41] C.T. Moynihan, S.K. Lee, M. Tatsumisago, T. Minami, Thermochim. Acta 280 (1996) 153.
[42] F. Kohlrausch, Pogg. Ann. Phys. 12 (1847) 393.
[43] G. Williams, D.C. Watts, Trans. Faraday Soc. 66 (1970) 80.
[44] O.S. Narayanaswamy, J. Am. Ceram. Soc. 54 (1971) 491.
[45] H. Vogel, Phys. Z. 22 (1921) 645.
[46] G.S. Fulcher, J. Am. Ceram. Soc. 8 (1923) 339.
[47] G. Tamman, W. Hesse, Z. Anorg. Allg. Chem. 156 (1926) 245.
[48] J.M. Hutchinson, A.J. Kovacs, J. Polym. Sci. Polym. Phys. Ed. 14 (1976) 1575.
[49] A.J. Kovacs, J.J. Aklonis, J.M. Hutchinson, A.R. Ramos, J. Polym. Sci. Polym. Phys. Ed. 17 (1979) 1097.

[50] J.M. Hutchinson, S. Montserrat, Thermochim. Acta 305 (1997) 257.
[51] M. Merzlyakov, C. Schick, Thermochim. Acta 330 (1999) 55.
[52] M. Merzlyakov, C. Schick, J. Therm. Anal. Cal. 61 (2000) 649.
[53] T. Vassiliev, unpublished data.
[54] H. Huth, M. Beiner, S. Weyer, M. Merzlyakov, C. Schick, E. Donth, this issue.
[55] A.A. Minakov, unpublished data.
[56] M. Merzlyakov, C. Schick, this issue.
[57] S.L. Simon, Macromolecules 30 (1997) 4056.
[58] L.C. Thomas, A. Boller, I. Okazaki, B. Wunderlich, Thermochim. Acta 291 (1997) 85.